 CMES, vol.64, no.1, pp.1-36, 2010

Higher-Order Stress-Strain Theory for Damage Modeling Implemented in an Element-free Galerkin Formulation

Yang Yang[1] **and Anil Misra**[2]

Abstract: Gradient theories have found wide applications in modeling of strain softening phenomena. This paper presents a higher order stress-strain theory to describe the damage behavior of strain softening materials. In contrast to most conventional gradient approaches for damage modeling, the present higher order theory considers strain gradients and their conjugate higher-order stress such that stable numerical solutions may be achieved. We have described the derivation of the required constitutive relationships, the governing equations and its weak form for this higher-order theory. The constitutive coefficients were obtained from a granular media approach such that the internal length scale parameter reflects the natural granularity of the underlying microstructure. The weak form was discretized using an element-free Galerkin (EFG) formulation that readily admits approximation functions of higher-order continuity. We have also discussed the implementation of essential boundary conditions and linearization of the derived discrete equations. Finally, the applicability of the derived model is demonstrated through two examples with different imperfections designed to initiate dislocation bands and shear bands, respectively.

Keywords: Higher-order stress, microstructure, granular materials, damage, strain softening, element-free Galerkin.

Introduction

A large number of engineering materials, such as concrete, rocks, polymers, ultrafine-grained metals and composites, exhibit strain softening behavior, which, often leads to a catastrophic material and structural failure. Materials undergoing strain softening gradually lose their load-carrying capacity accompanied by increasingly localized deformations as those documented by many researchers (van Mier 1984, 1986;

[1] Faculty of Engineering, China University of Geosciences, Wuhan, 430074, China.
[2] Civil, Environmental and Architectural Engineering Department, The University of Kansas, KS, USA. Tel.: (785) 864-1750, Fax: (785) 864-5631, E-mail: amisra@ku.edu

van Mier, et.al. 1997; Sluys, Cauvern and de Borst 1995). It is now widely recognized that the tangential moduli for these materials ceases to be positive-definite upon onset of strain softening, resulting in a set of ill-posed partial differential equations(PDE) whose solutions may have no physical significance. The consequence of such a stress-strain relationship is that the traditional finite element solutions based upon classical continuum description become powerless. For instance, when strain softening of materials is treated as classical elasticity or elastoplasticity problem, their finite-element solutions suffer from numerical instabilities and severe mesh sensitivity (Pietruszczak and Mroz 1981; Bažant, Belytschko and Chang 1984; Sandler 1984; Frantziskonis and Desai 1987; de Borst, Sluys, Mühlhaus and Pamin 1993; Chen, Wu and Belytschko 2000). In addition, the solutions become physically unrealistic with increasing mesh refinement, since the energy dissipated in the strain-softening domain tends to zero as the strain localizes into a single element (Bažant 1976; Nemes and Spéciel 1996).

Four alternative approaches have been suggested in the literature to remedy the above mentioned numerical deficiencies of the classical continuum model. These so-called regularization techniques are generally based on the enrichment of the classical continuum description with additional terms. One alternative is to utilize the micropolar theory (or the more well known Cosserat theory) which considers an additional material rotational degree of freedom independent from the displacement field (Mindlin 1969; Chang and Ma 1990; Fleck and Hutchinson 1993; Steinmann 1994; Chang, Wang, Sluys and van Mier 2002a, b). A second alternative is to incorporate rate dependence or viscous effects within the constitutive models (Sandler 1984; Wu and Freund 1984; Needleman 1988; Sluys and de Borst 1992; Nemes and Spéciel 1996). The third alternative is to use non-local theory proposed originally by Kroner (1967) and applied to strain-softening by Bažant, Belytschko and Chang (1984) in which stresses and strains at a given point depend on a convolution type integral accounting for the history of displacements in a finite neighborhood about the point in question (Chen, Wu and Belytschko 2000; Murakami, Kendall, and Valanis 1993; Valanis 1991; Bažant and Pijaudier-Cabot 1988; Belytschko, Bažant, Hyun and Chang 1986; de Vree, Brekelmans and van Gils 1995).

The above three alternatives have been reported to have different capabilities to describe strain softening either in static or dynamic problems. A fourth alternative, followed in this paper, is the addition of higher-order gradients in the system governing equations. Among the attractions of this approach are its simplicity as no rotational degree of freedom or time effects are required, nor is there any dependence on unknown 'weak zones' within the solid, and the difficult to determine influence functions for the convolution integrals appearing in the classical non-local models are avoided (Triantafyllidis and Bardenhagen 1993). In addition, this approach fol-

lows strict locality in a mathematical sense (Peerlings, de Borst, Brekelmans and de Vree 1996) and incorporates an inherent characteristic length scale that determines the size of the localization zone. This type of models can be further divided into two categories: (i) in which only the higher order strains are considered, and (ii) the more rigorous type in which both higher-order strain and higher-order stress gradients are considered.

The first type of gradient model has been widely used for: (i) investigating softening failure behavior in the context of plasticity (de Borst and Mühlhaus 1992; Pamin 1994; de Borst, Pamin, Peerlings and Sluys 1995) and in the context of elasticity (Peerlings, de Borst, Brekelmans and de Vree 1996; Altan and Aifantis 1997; Chang, Askes and Sluys 2002); and (ii) analyzing elastic wave propagation (Sluys 1992; Sluys, de Borst and Mühlhaus 1993; Chang and Gao 1997; Chang, Gao and Zhong 1998; Suiker, de Borst and Chang 2001a,b). Models with strain gradients can overcome one of the major shortcomings in constitutive equations for solids admitting localization of deformation at finite strains, i.e. their inability to provide physically acceptable solutions to boundary value problems in the post-localization range due to loss of ellipticity of the governing equations (Triantafyllidis and Aifantis 1986). However, a peculiar characteristic of this type of models is that the discrete tangent stiffness does not maintain positive definiteness resulting in the numerical difficulties associated with strain-softening (Chang, Askes and Sluys 2002).

In contrast, the second type of gradient-enhanced model contains both the higher-order strain and the higher-order stress terms. This type of model appears to unconditionally maintain the stability and, therefore, offers a more robust approach. However, this approach has been rarely employed mainly because of its numerical complexity. Chang, Askes and Sluys (2002) compared the performances of the higher-order gradient models with and without higher-order stress for modeling fracture behavior in the context of an infinitely long bar. They concluded that the addition of higher-order stress terms results in stabilizing the positive definiteness of the tangent stiffness moduli when entering the strain softening regime such that physically significant solutions can be ensured and strain-softening phenomenon can be realistically reproduced. The present work builds upon the success of this higher-order stress-strain theory in dealing with one-dimensional strain softening problem by Chang and coworkers (2002) and further develops the approach for multi-dimensional simulation of localized failure process.

In this paper, we focus upon the derivation of a first-order theory that includes the usual Cauchy stresses and strains termed as zeroth-order tensors in constitutive model, and the first-order gradient of strain and its conjugated first-order stress. All the formulations are derived using the tensor notations such that they can be readily

applied to multi-dimensional analysis. We derive the higher-order constitutive laws on the basis of a microstructural mechanics approach used for modeling granular media (Chang and Gao 1995; Mühlhaus and Oka 1996; Suiker, de Borst and Chang 2001a,b). We postulate that a monolithic material can be represented as a granular material with a certain material packing structure. The macroscopic material model of this pseudo-granular material is obtained in terms of the microscopic material properties. For simplicity, an isotopic granular packing structure is utilized. As a result, first-order gradient damage constitutive models are derived such that a so-called internal length scale, i.e. the particle radius, is incorporated directly into the model to reflect the granularity of the underlying microstructure. We then derive the governing equations and their weak form for this first-order gradient theory and solve them using meshfree techniques.

Meshfree methods, such as the EFG (Belytschko, Lu and Gu 1994) method and the Meshless Local Petrov-Galerkin (MLPG) method (Atluri, and Shen 2002) have been used as an alternative to eliminate the mesh-subjectivity. The EFG method, known to require a set of much looser topological background cells for numerical integrations of the global weak form compared to FEM, has been demonstrated to be quite successful in solving many challenging problems in solid mechanics, for instance, static and dynamic crack growth modeling (Krysl and Belytschko 1997; Belytschko and Tabbara 1996; Belytschko, Lu and Gu 1994, 1995; Belytschko, Lu, Gu and Tabbara 1995; Belytschko, Gu and Lu 1994; Lu, Belytschko and Tabbara 1994). The MLPG method, in which the weak form of equilibrium equations are based on a local sub-domains such that it involves neither elements for interpolation nor shadow meshes for integration, has also been applied widely to solid mechanics problems (Atluri and Zhu 1998; Atluri, and Shen 2002), including to the Toupin-Mindlin formulation of strain gradient theories in 2-D elasticity context (Tang, Shen and Atluri 2003). However, there have been only few attempts to apply the EFG or the MLPG method to gradient-enhanced continua with strain softening (Askes, Pamin and de Borst 2000; Chang, Askes, Sluys 2002) or in the context of plasticity (Pamin, Askes and de Borst 2001, 2003). Jirásek (1998) has investigated the applicability of EFG method to strain softening problems and confirmed that for regularized localization problems EFG method behaves in a manner superior to finite element (FE) method in the description of continuous fields. From the viewpoint of gradient-enhanced continuum theory developed in this paper, the EFG or the MLPG method has an important advantage over classical FEM that the approximation functions with high order of continuity needed for proper representation of the higher-order derivatives can be readily incorporated into the formulation without increasing the problem size (Askes, Pamin and de Borst 2000; Pamin, Askes and de Borst 2003).

In the subsequent sections, we first derive the first-order constitutive equations that incorporate an elastic damage law utilizing a discrete granular packing. We then discuss the derivation of the system equilibrium equation based on an energy approach as well as the enforcement of essential boundary conditions using penalty method. The EFG formulation is then presented, which includes a brief review of the moving least square (MLS) approximation, the discretization and linearization procedure to arrive at the final incremental form of the governing equation. Finally, two examples in 2-D with different imperfections under displacement-controlled uniaxial tension are numerically analyzed to demonstrate the applicability of the proposed higher-order gradient model for modeling strain-softening behavior.

1 Higher-order stress/strain damage model

1.1 Damage law

Upon applying an isotropic damage law, the classical constitutive relation becomes (Askes, Pamin, and de Borst 2000; Peerlings, de Borst, Brekelmans and de Vree 1996; de Vree, Brekelmans and van Gils 1995)

$$\sigma = (1-\omega)D\varepsilon \tag{1}$$

where ω is the so-called damage scalar quantity ranging from 0 for initial undamaged material to 1 when all material coherence is lost. D is the elastic moduli with σ and ε the Cauchy stress tensor and the corresponding strain tensor, respectively. For the example calculations in this paper, the damage state is governed by a linear strain softening damage law through a scalar state variable, k, defined as the overall effective strain. The effective strain, k, is determined by the square root of the summation of principle strains considering damage due to only tensile strains, which, in 2-D, is given by the following equation

$$k = \sqrt{(\varepsilon_1)^2 + (\varepsilon_2)^2} \text{ for } \varepsilon_1, \varepsilon_2 > 0 \tag{2}$$

where ε_1 and ε_2 are the principal strain components of strain $\varepsilon = \begin{bmatrix} \varepsilon_{11} & \varepsilon_{12} \\ \varepsilon_{12} & \varepsilon_{22} \end{bmatrix}$.
The linear softening damage evolution function takes the form

$$\omega(k) = \begin{cases} \frac{k_u(k-k_0)}{k(k_u-k_0)} & k_0 \le k \le k_u \\ 1 & k > k_u \end{cases} \tag{3}$$

where k_0 is the threshold of strain at which damage is initiated and k_u is the strain level at which all load carrying capacity is exhausted.

1.2 Formulation of higher-order constitutive law using microstructural approach

A macroscopic continuum is postulated to have a granular microstructure consisting of a set of interacting particles whose centroids represent material points as depicted in Fig. 1. Under an applied load on a sample of such a material, the conceptual grains may undergo translation or rotation. The relative displacement, δ_i, between two nearest neighbor particles n and p (see Fig. 1) (Chang and Misra 1990) is given by

$$\delta_i = u_i^n - u_i^p + e_{ijk}(\omega_j^n r_k^n - \omega_j^p r_k^p) \tag{4}$$

where u_i =particle displacement; ω_j =particle rotation; r_k = vector joining the centroid of particle to the contact point; superscripts refer to the interacting particles; e_{ijk} =the permutation symbols. Note that all subscripts follow the summation convention of tensor unless stated otherwise.

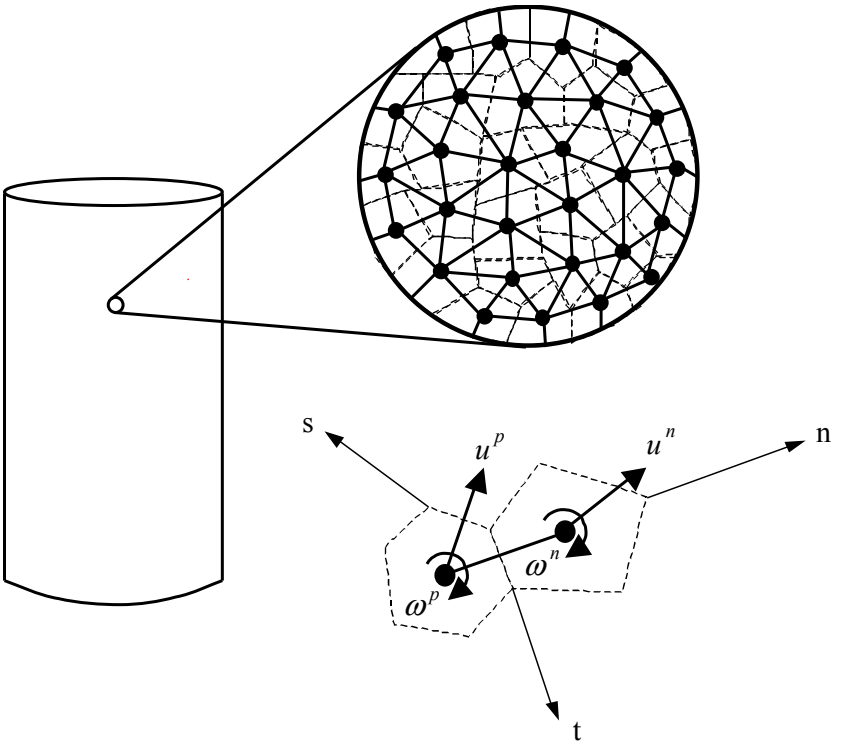

Figure 1: Conceptual granular model of a continuum

The contact force f_i^c between two particles may be related to the relative displace-

ment δ_j^c through the contact stiffness K_{ij}^c as

$$f_i^c = K_{ij}^c \delta_j^c \tag{5}$$

with K_{ij}^c written in terms of the stiffness components in the normal direction K_n and that in the tangential direction $K_w$as

$$K_{ij}^c = K_n^c n_i n_j + K_w^c (s_i s_j + t_i t_j) \tag{6}$$

where n, s, t are the unit base vectors of the local coordinate system constructed at each contact as shown in Fig. 2. Vector n is normal to the contact plane and the other two orthogonal vectors, s and t, are on the contact plane which are given by

$$\begin{cases} n = \cos\gamma e_1 + \sin\gamma\cos\psi e_2 + \sin\gamma\sin\psi e_3 \\ s = \frac{dn}{d\gamma} = -\sin\gamma e_1 + \cos\gamma\cos\psi e_2 + \cos\gamma\sin\psi e_3 \\ t = n \times s = -\sin\psi e_2 + \cos\psi e_3 \end{cases} \tag{7}$$

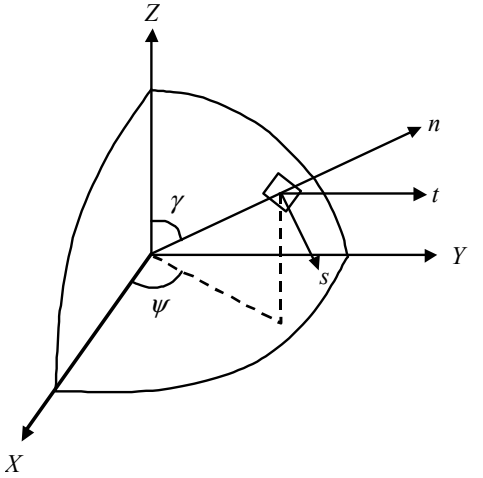

Figure 2: Local coordinate system at an inter-particle contact

The strain energy density in a representative volume V can be written as

$$W = \frac{1}{2V} \sum_{c=1}^{N} f_i^c \delta_i^c \tag{8}$$

with N refers to the total number of inter-particle contacts in the representative volume V. To develop a continuum model for the behavior of a particle assembly, it is

desirable to equate the discrete displacement u_i^n of nth particle to the displacement at the centroid of the nth particle, that is

$$u_i(x_i^n) = u_i^n \tag{9}$$

with x_i^n the coordinate of centroid of the particle$n$.

Following the approach by Chang and Liao (1990), Taylor series expansions is used for the displacement field. Thus, the displacement at particle n can be estimated using the gradients at a reference point, x^0, which is defined as the center of the representative volume as follows:

$$u_i(x^n) = u_i(x^0) + u_{i,j}(x^0)x_j + \frac{1}{2}u_{i,jk}(x^0)x_j x_k \tag{10}$$

where the third-order derivatives and higher are neglected Ignoring the inter-particle rotations, i.e. assuming a class of non-polar type of continua (Chang and Gao 1995), and substituting Eq. (10) into Eq. (4) we get

$$\delta_i^c = u_i(x^n) - u_i(x^p) = u_{i,j}L_j^c + u_{i,jk}J_{jk}^c \tag{11}$$

where the geometric quantities

$$L_j^c = x_j^n - x_j^p \tag{12a}$$

$$J_{jk}^c = \frac{1}{2}(x_j^n x_k^n - x_j^p x_k^p) \tag{12b}$$

Assuming a uniform particle radius r and the origin of local coordinates is located at the pth particle, then Eqs. (12a)-(12b) are equivalent to

$$L_j^c = 2rn_j^c \tag{13a}$$

$$J_{jk}^c = \frac{1}{2}L_j^c L_k^c \tag{13b}$$

Substituting Eqs. (5) and (11) into Eq. (8) yields

$$W = \frac{1}{2V}\sum_{c=1}^{N}(K_{iq}^c \delta_q^c L_j^c u_{i,j} + K_{iq}^c \delta_q^c J_{jk}^c u_{i,jk}) \tag{14}$$

Let the strain measure ε be written as

$$\varepsilon_{ij}^0 = u_{i,j} \quad \varepsilon_{ijk}^I = u_{i,jk} \tag{15}$$

Then the stress measures σ can be defined as

$$\sigma^0_{ij} = \frac{\partial W}{\partial \varepsilon^0_{ij}} \quad \sigma^I_{ijk} = \frac{\partial W}{\partial \varepsilon^I_{ijk}} \tag{16}$$

By combining Eqs. (11), (13a)-(16), following set of constitutive equations is found:

$$\sigma^0_{ij} = C_{ijqm}\varepsilon^o_{qm} + B_{ijqmn}\varepsilon^I_{qmn} \tag{17a}$$

$$\sigma^I_{ijk} = B_{ijkqm}\varepsilon^0_{qm} + D_{ijkqmn}\varepsilon^I_{qmn} \tag{17b}$$

where the constitutive tensors are expressed in terms of the fabric measures as

$$C_{ijqm} = \frac{1}{2V}\sum_{c=1}^{N} L^c_j K^c_{iq} L^c_m \tag{18a}$$

$$B_{ijqmn} = \frac{1}{4V}\sum_{c=1}^{N} L^c_j K^c_{iq} L^c_m L^c_n \tag{18b}$$

$$D_{ijkqmn} = \frac{1}{8V}\sum_{c=1}^{N} L^c_j L^c_k K^c_{iq} L^c_m L^c_n \tag{18c}$$

In the present study, only zeroth-order and first-order strains, ε^0_{ij}, ε^I_{ijk} and their conjugate stresses, σ^0_{ij}, σ^I_{ijk} are considered. Assuming the central symmetry of material, the constitutive tensor B_{ijqmn}=0 as stated by Chang, Askes, and Sluys (2002), and the constitutive equations are further simplified to:

$$\sigma^0_{ij} = C_{ijkl}\varepsilon^0_{kl} \tag{19a}$$

$$\sigma^1_{ijq} = D_{ijqklm}\varepsilon^1_{klm} \tag{19b}$$

Since the representative volume consists of a large number of particles, a summation of any quantity over all particle contacts within the volume can be expressed in an integral form by introducing a directional density function in terms of spherical harmonic expansions which represents the discrete distribution of inter-granular interactions in a continuum manner (Chang and Misra 1990). A truncated form of spherical harmonic expansions is employed herein as

$$\xi(\gamma,\psi) = \frac{1}{4\pi}[1 + \frac{1}{4}a_{20}(3\cos 2\gamma + 1) + 3\sin^2\gamma(a_{22}\cos 2\psi + b_{22}\sin 2\psi)] \tag{20}$$

With the fabric parameters a_{20}, a_{22} and b_{22} determining the anisotropy of the material. For a suitably large representative volume with a large number of contacts,

recalling Eq. (13a), the summation in Eqs. (18a) and (18c) may be recast into integral forms as

$$C_{ijkl} = \frac{2r^2 N}{V} \int_{\Omega} n_j^c K_{ik}^c n_l^c \xi(\gamma, \psi) d\Omega \tag{21a}$$

$$D_{ijqklm} = \frac{2r^4 N}{V} \int_{\Omega} n_j^c n_q^c K_{ik}^c n_l^c n_m^c \xi(\gamma, \psi) d\Omega \tag{21b}$$

where the integration $\int_{\Omega}(\quad) d\Omega = \int_0^{2\pi}\int_0^{\pi}(\,)\sin\gamma d\gamma d\psi$; and $N\xi(\gamma,\psi)d\Omega$= the number of contacts in the interval Ω to $\Omega + d\Omega$. Considering the symmetry of the higher-order stress and strain tensors, the fourth-rank and sixth-rank constitutive tensors have to satisfy the following symmetries

$$C_{ijkl} = C_{klij} \tag{22}$$

$$D_{ijqklm} = D_{klmijq} \tag{23}$$

Appendix A gives the closed form expressions for the constitutive coefficients of an isotropic material in terms of the Young's modulus, Poisson's ratio and the particle size.

In a damage context we assume that all constitutive coefficients are pre-multiplied with the same factor $(1-\omega)$ such that a nonlinear higher-order constitutive damage model can be obtained as:

$$\sigma_{iq}^0 = (1-\omega) C_{iqkl} \varepsilon_{kl}^0 \tag{24a}$$

$$\sigma_{ijq}^1 = (1-\omega) D_{ijqklm} \varepsilon_{klm}^1 \tag{24b}$$

2 Derivation of system equilibrium equation

2.1 Energy functional and weak form

Following the framework for strain-gradient theory (Fleck and Hutchinson 1997), the strain potential energy density with higher-order stress can be expressed as

$$W = \int_{\varepsilon^0} \sigma_{iq}^0 d\varepsilon_{iq}^0 + \int_{\varepsilon^1} \sigma_{ijq}^1 d\varepsilon_{ijq}^1 \tag{25}$$

To proceed, we substitute the damage constitutive relations from Eqs. (24a) and (24b) into Eq. (25) and make use of integration by parts for the higher-order term

while ignoring the boundary terms such that the final form of the energy functional can be recast as

$$W = \int_{\varepsilon^0}(1-\omega)C_{iqkl}\varepsilon^0_{kl}d\varepsilon^0_{iq} - \int_{\varepsilon^0}(1-\omega)D_{ijqklr}\frac{\partial^2\varepsilon_{kl^0}}{\partial x_r\partial x_j}d\varepsilon^0_{iq} + \int_{\varepsilon^0}\frac{\partial\omega}{\partial\varepsilon_{mn^0}}\frac{\partial\varepsilon_{mn^0}}{\partial x_j}D_{ijqklr}\frac{\partial\varepsilon^0_{kl}}{\partial x_r}d\varepsilon^0_{iq} \quad (26)$$

where the substitution $\varepsilon^I_{ijq} = \partial\varepsilon^0_{iq}/\partial x_j$ has been used. Stationarity of the potential energy is investigated by minimizing Eq. (26) which results in the following nonlinear equilibrium equation in terms of displacement gradients:

$$\begin{aligned}&(1-\omega)[C_{iqkl}\frac{\partial^2u_k}{\partial x_q\partial x_l} - D_{ijqklr}\frac{\partial^4u_k}{\partial x_r\partial x_j\partial x_q\partial x_l}]\\ &-\frac{\partial\omega}{\partial\varepsilon^0_{mn}}\frac{\partial^2u_m}{\partial x_q\partial x_n}[C_{iqkl}\frac{\partial u_k}{\partial x_l} - D_{ijqklr}\frac{\partial^3u_k}{\partial x_r\partial x_j\partial x_l}]\\ &+\frac{\partial\omega}{\partial\varepsilon^0_{mn}}D_{ijqklr}[\frac{\partial^3u_m}{\partial x_j\partial x_q\partial x_n}\frac{\partial^2u_k}{\partial x_r\partial x_l} + \frac{\partial^2u_m}{\partial x_j\partial x_n}\frac{\partial^3u_k}{\partial x_r\partial x_q\partial x_l}] = 0 \quad (27)\end{aligned}$$

Next, Galerkin method is utilized to derive the weak form equilibrium equation. Pre-multiplying Eq. (27) by a test function δu_i and integrating over the 2-D domain Ω, the weak form governing equation is obtained as

$$\int_\Omega\frac{\partial\delta u_i}{\partial x_q}(1-\omega)C_{iqkl}\frac{\partial u_k}{\partial x_l}dxdy + \int_\Omega\frac{\partial^2\delta u_i}{\partial x_q\partial x_j}(1-\omega)D_{ijqklr}\frac{\partial^2u_k}{\partial x_r\partial x_l}dxdy = \int_{\Gamma_t}\frac{\partial\delta u_i}{\partial x_q}\sigma^1_{ijq}n_jd\Gamma + \int_{\Gamma_t}\delta u_i(\sigma^0_{iq} - \frac{\partial\sigma^1_{ijq}}{\partial x_j})n_qd\Gamma \quad (28)$$

Appendix B gives the details of the above derivation. The right-hand side of Eq.(28) includes boundary integrals representing the boundary conditions. According to Reddy (2005), terms corresponding to the test function in the boundary integrals are determined as the essential boundary conditions, while their coefficients form the natural boundary conditions. Thus, the boundary conditions for this higher-order equilibrium system can be stated as

Essential b.c.: u_i specified, $u_{i,q}$ specified (29a)

Natural b.c.: $\sigma^0_{iq} - \dfrac{\partial\sigma^1_{ijq}}{\partial x_j}$ specified, σ^1_{ijq} specified (29b)

Note that though boundary conditions have been distinguished, the physical significance of the natural boundary conditions resulting from higher-order stresses remains an open question.

2.2 Enforcement of essential boundary conditions using penalty method

The natural boundary conditions (or traction boundary conditions) have been included into the weak form equilibrium equation via integration by parts. However, the essential boundary conditions (or displacement boundary conditions) have not yet been treated in the formulation. Moreover, the MLS approximations used latter in EFG discretizaiton do not bear the Kronecker delta function property. Therefore, the essential boundary conditions have to be imposed separately via special techniques, such as the Lagrange multiplier method and the penalty method. However, it is well-known that the Lagrange multiplier method increases the number of field variables and the resultant dimensions of the system matrix such that the computational costs are unavoidably raised. In addition, the Lagrange multiplier method results in a loss of the positive-definiteness of system matrix. In contrast, the penalty method offers a more efficient way to impose the essential boundary conditions without increasing the number of unknowns provided an appropriate large penalty coefficient is utilized. Zhu and Atluri (1998) have presented a penalty formulation of the EFG method which was verified through two benchmark closed-form problems, namely a cantilever beam and an infinite plate with a circular hole. Their results indicated that the penalty method yields a banded, symmetric and positive definite system matrix and does not exhibit any volumetric locking while retaining high rates of convergence for both displacements and strain energy. The constrained higher-order Galerkin weak form (Eq. (28)) using penalty method is posed as follows (Liu and Gu 2005):

$$\int_\Omega \frac{\partial \delta u_i}{\partial x_q}(1-\omega)C_{iqkl}\frac{\partial u_k}{\partial x_l}dxdy + \int_\Omega \frac{\partial^2 \delta u_i}{\partial x_q \partial x_j}(1-\omega)D_{ijqklr}\frac{\partial^2 u_k}{\partial x_r \partial x_l}dxdy$$
$$- \int_{\Gamma_t} \frac{\partial \delta u_i}{\partial x_q}\sigma^1_{ijq}n_j d\Gamma - \int_{\Gamma_t} \delta u_i(\sigma^0_{iq} - \frac{\partial \sigma^1_{ijq}}{\partial x_j})n_q d\Gamma$$
$$- \frac{1}{2}\int_{\Gamma_u} \delta[(u_i-\bar{u}_i)^T \alpha(u_i-\bar{u}_i)]d\Gamma = 0 \quad (30)$$

where $\bar{u}_i$ is the prescribed displacement vector; α is the penalty coefficient which is often a large positive number and is determined herein by 10^6 times the maximum diagonal element of the global stiffness matrix K. In Eq. (30), the higher-order essential boundary conditions are ignored for the sake of simplicity, though it could be included in an obvious and straightforward manner. Considering that

$$\frac{1}{2}\int_{\Gamma_u} \delta[(u_i-\bar{u}_i)^T \alpha(u_i-\bar{u}_i)]d\Gamma = \int_{\Gamma_u} \delta u_i^T \alpha u_i d\Gamma - \int_{\Gamma_u} \delta u_i^T \alpha \bar{u}_i d\Gamma \quad (31)$$

Eq.(30) can be recast as

$$\int_\Omega \frac{\partial \delta u_i}{\partial x_q}(1-\omega)C_{iqkl}\frac{\partial u_k}{\partial x_l}dxdy+\int_\Omega \frac{\partial^2 \delta u_i}{\partial x_q \partial x_j}(1-\omega)D_{ijqklr}\frac{\partial^2 u_k}{\partial x_r \partial x_l}dxdy$$
$$-\int_{\Gamma_u}\delta u_i^T \alpha u_i d\Gamma=\int_{\Gamma_t}\frac{\partial \delta u_i}{\partial x_q}\sigma^1_{ijq}n_j d\Gamma+\int_{\Gamma_t}\delta u_i(\sigma^0_{iq}-\frac{\partial \sigma^1_{ijq}}{\partial x_j})n_q d\Gamma$$
$$-\int_{\Gamma_u}\delta u_i^T \alpha \bar{u}_i d\Gamma=0 \quad (32)$$

3 Element-free Galerkin Formulation

3.1 MLS approximation

The essential idea for EFG method is that MLS interpolants are used for the trail and test functions with a variational principle. To use MLS, it is only necessary to construct a set of nodes in the problem domain without any elements. The connectivity between field nodes is satisfied via the overlapping of the domain of influence of sampling node in which its shape function is nonzero. The domain of influence of each field node is controlled by a weight function $w_i(x)$ which is the product of standard 1D weight functions in x and y directions for 2-D case expressed as

$$w_i(x)=w_{ix}(x)\cdot w_{iy}(x) \quad (33)$$

In this study, a cubic spline is used as the weight function and the domain of influence is set to be rectangular with dimensiond_{sx} and d_{sy} which are determined by a dimensionless parameter β and the nodal spacing d_{cx} and d_{cy} in each direction respectively. For instance, the weight function in x direction takes the following form

$$w_{ix}(x)=\begin{cases}2/3-4\bar{r}_{ix}^2+4\bar{r}_{ix}^3 & \bar{r}_{ix}\le 0.5\\ 4/3-4\bar{r}_{ix}+4\bar{r}_{ix}^2-4/3\bar{r}_{ix}^3 & 0.5<\bar{r}_{ix}\le 1\\ 0 & \bar{r}_{ix}>1\end{cases} \quad (34)$$

where $\bar{r}_{ix}=\frac{|x-x_i|}{d_{sx}}$, $d_{sx}=\beta d_{cx}$ (with $\beta=3$) and $|x-x_i|$ is the distance from node x_i to the sampling point x.

The MLS approximation $u^h(x)$ for displacement field function $u(x)$ at x is defined as

$$u^h(x)=\Phi^T(x)U_s \quad (35)$$

where U_s is the vector collecting the nodal parameters of displacement field for all the nodes within the influence domain; $\Phi^T(x)$ is the vector of MLS shape functions

corresponding to n nodes in the influence domain of the sampling point x, written as

$$\Phi^T(x) = \{\varphi_1(x)\ \varphi_2(x)\ \cdots\ \varphi_n(x)\}_{1\times n} = p^T(x)A^{-1}(x)B(x) \tag{36}$$

where the polynomial base vector p takes the quadratic form as

$$p^T(x) = [1\ x\ y\ x^2\ xy\ y^2] \tag{37}$$

and the matrix $A(x)$ and vector $B(x)$ are given as

$$A(x) = \sum_{i=1}^{n} w_i(x)p(x_i)p^T(x_i) \tag{38}$$

$$B(x) = [w_1(x)p(x_1)\ \ w_2(x)p(x_2)\ldots\ \ w_n(x)p(x_n)] \tag{39}$$

3.2 Discretization and Linearization

The trial function and test function are discretized according to:

$$u_i = \varphi_{ip}u_p\ \ \delta u_i = \varphi_{ip}\delta u_p. \tag{40}$$

In which φ_{ip} is the MLS shape function and u_p is the nodal parameter of displacement field for all nodes in the influence domain. Substituting Eq. (40) into the weak form Eq. (32) and canceling out δu_p because of its arbitrariness yields the following global discretized system equation

$$[K_{ps} + K_{ps}^{\alpha}]u_s = F_p + F_p^{\alpha} \tag{41}$$

where superscript α represents the resultants from penalty terms. Global stiffness tensors K_{ps}, K_{ps}^{α} and global force tensors F_p, F_p^{α} are given as

$$K_{ps} = \int_{\Omega} \frac{\partial \varphi_{ip}^T}{\partial x_q}(1-\omega)C_{iqkl}\frac{\partial \varphi_{ks}}{\partial x_l}dxdy + \int_{\Omega} \frac{\partial^2 \varphi_{ip}^T}{\partial x_q \partial x_j}(1-\omega)D_{ijqklr}\frac{\partial^2 \varphi_{ks}}{\partial x_r \partial x_l}dxdy \tag{42}$$

$$K_{ps}^{\alpha} = -\int_{\Gamma_u} \varphi_{ip}^T \alpha \varphi_{is} d\Gamma \tag{43}$$

$$F_p = \int_{\Gamma_t} \frac{\partial \varphi_{ip}^T}{\partial x_q}\sigma_{ijq}^1 n_j d\Gamma + \int_{\Gamma_t} \varphi_{ip}^T(\sigma_{iq}^0 - \frac{\partial \sigma_{ijq}^1}{\partial x_j})n_q d\Gamma \tag{44}$$

$$F_p^{\alpha} = -\int_{\Gamma_u} \varphi_{ip}^T \alpha \bar{u}_i d\Gamma \tag{45}$$

In order to obtain the incremental form of system Eq. (41), we define a residual force R_p as the difference between internal force $(K_{ps}+K_{ps}^{\alpha})u_s$ and external force $F_p+F_p^{\alpha}$. Taylor series expansion of the residual force is then utilized to perform the linearization given by

$$R_p = R_p(u^{(r-1)}) + (\frac{\partial R_p}{\partial u_s})^{(r-1)}\Delta u_s^{(r)} + \frac{1}{2}(\frac{\partial^2 R_p}{\partial u_s^2})^{(r-1)}(\Delta u_s^{(r)})^2 \cdots = 0 \tag{46}$$

where $\Delta u^{(r)}$ is the increment and superscripts within parentheses refer to the iteration step. Thus the solution of Eq. (41) at the rth iteration can be written in terms of the solution for the $(r-1)$th iteration as follows

$$u^{(r)} = u^{(r-1)} + \Delta u^{(r)} \tag{47}$$

When second-order derivatives and higher in Eq. (46) are neglected, we obtain

$$(\frac{\partial R_p}{\partial u_s})^{(r-1)}\Delta u_s^{(r)} = F_p + F_p^{\alpha} - (K_{ps}^{(r-1)} + K_{ps}^{\alpha(r-1)})u_s^{(r-1)} \tag{48}$$

Defining tangent stiffness as $T_{ps} = \frac{\partial R_p}{\partial u_s}$ yields

$$T_{ps} = \sum_{m=1}^{n} \frac{\partial (K_{pm}+K_{pm}^{\alpha})}{\partial u_s} u_m + (K_{ps}+K_{ps}^{\alpha}) \tag{49}$$

Inserting Eq. (42) and Eq. (43) into Eq. (49), the resultant tangent stiffness tensor is obtained as

$$\begin{aligned} T_{ps} = &\int_{\Omega} \frac{\partial \varphi_{ip}^T}{\partial x_q}(1-\omega)C_{iqkl}\frac{\partial \varphi_{ks}}{\partial x_l}dxdy + \int_{\Omega} \frac{\partial^2 \varphi_{ip}^T}{\partial x_q \partial x_j}(1-\omega)D_{ijqklr}\frac{\partial^2 \varphi_{ks}}{\partial x_r \partial x_l}dxdy \\ &- \int_{\Gamma_u} \varphi_{ip}^T \alpha \varphi_{is} d\Gamma - \int_{\Omega} \frac{\partial \varphi_{ip}^T}{\partial x_q}\frac{\partial \omega}{\partial \varepsilon_{ab}^0}\frac{\partial \varphi_{as}}{\partial x_b}C_{iqkl}\varepsilon_{kl}^0 dxdy \\ &- \int_{\Omega} \frac{\partial^2 \varphi_{ip}^T}{\partial x_q \partial x_j}\frac{\partial \omega}{\partial \varepsilon_{ab}^0}\frac{\partial \varphi_{as}}{\partial x_b}D_{ijqklr}\frac{\partial \varepsilon_{kl}^0}{\partial x_r}dxdy \end{aligned} \tag{50}$$

Finally, the incremental system equilibrium equation becomes

$$T_{ps}^{(r-1)}\Delta u_s^{(r)} = F_p + F_p^{\alpha} - (K_{ps}^{(r-1)} + K_{ps}^{\alpha(r-1)})u_s^{(r-1)} \tag{51}$$

4 Numerical example

A majority of published work on the simulation of strain softening using higher-order gradient models employ a one-dimensional bar model under uniaxial tension which has an imperfection in the middle to trigger the localization(de Borst, Pamin, Peerlings and Sluys 1995; Peerlings, de Borst, Brekelmans and de Vree 1996; Chang, Askes and Sluys 2002). To validate the applicability of the higher-order stress/strain models implemented in an EFG formulation for simulating multi-dimensional problems, we have presented two examples of 2-D models with different types of imperfections.

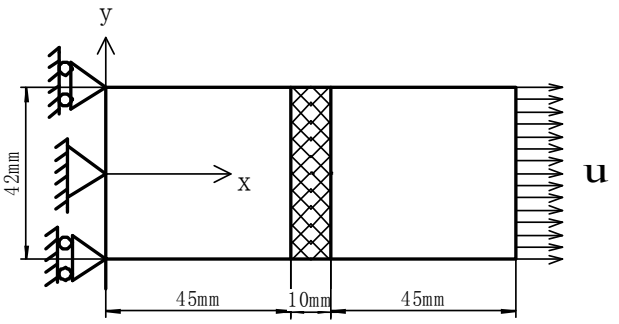

Figure 3: Plate with an imperfect zone parallel to a section – geometry and loading conditions

4.1 Example 1 – Plate with an imperfect zone parallel to a section

We consider a rectangular 2-D domain (length=100mm, width=42mm) subjected to a uniaxial tension via an incrementally imposed displacement Δu=0.0025mm at the right end while the left end is fixed at the upper and lower vertices and the center point with hinged joint as shown in Fig. 3. To initiate a localization band, a 10mm wide imperfection zone, shown as the hatched area in Fig. 3, is considered along the center section of the domain. Such an imperfection would represent the inter-granular glassy films often observed in ceramic materials (Misra, Ouyang, Chen and Ching 2007). The imperfection is characterized by a 10% reduction of material property in terms of Young's modulus which is taken as E=2×10^{4}N/mm^2 for the plate material. Poisson's ratio is taken as ν=0.25, and the damage evolution parameters are given as k_0=10^{-4} and k_u=0.0125. A 33×13 uniform nodal layout is used for obtaining the solutions for this problem. In addition, 14×8 rectangular background cells with four-point integration rule are used to integrate the stiffness coefficient. The internal length scale parameter is taken as$r$=1.5mm. The

incremental displacement is imposed in thirteen stages until the plate completely fractures.

4.1.1 Example 1 – Evolution of damage and strain localization

Fig. 4 shows the computed contours of axial strain ε_{11} and stress σ_{11} in horizontal direction (x direction) at three stages, namely, pre-peak, peak and failure stages. The three stages correspond to the overall stretch u=0.01, 0.0125, 0.0325mm. In the pre-peak nonlinear stage shown in Fig. 4(a), the imperfection has triggered damage development in the central zone such that it enters strain softening mode leading to a primitive localization band. At this stage, the strain in the region outside the imperfection is strictly uniform and remains unchanged during the subsequent loading. This is also reflected in the stress contour in the right column of Fig. 4(a) where a distinct weak zone of $\sim$7mm width appears. Upon further loading, the strain localization band expands to $\sim$20mm wide at peak stress as shown in Fig. 4(b). Subsequently, the width of the softening band remains constant until the final rupture shown in Fig. 4(c). We observe from the stress contour in Fig. 4(c) that the axial stress σ_{11} in the weak zone reduces by about 17% compared to the peak stress revealing an unloading phenomenon.

The contours of strain ε_{22} and stress σ_{22} corresponding to the previous three stages are plotted in Fig. 5. As the damage develops in the central zone, lateral strain ε_{22} localizes as well beginning from the outer edge of the plate. This behavior is expected as the material contracts laterally when the imperfection experiences increasing tensile strains in the horizontal direction. Naturally, the free edges undergo larger contraction than the internal locations, such that the structure retains a partial load carrying capacity until the last stage shown in the Fig. 5(c). Thus, the lateral strain localization forms two separate weak zones at the upper and lower edges of the imperfection that progress inwards.

Fig. 6 plots the development of the overall effective strain and stress contours at the peak and failure stages. The overall effective strain is obtained according to Eq. (2) which is defined as the square root of the summation of the principle strain components. Similarly, the overall effective stress $\bar{\sigma}$ can be calculated according to

$$\bar{\sigma} = \sqrt{(\sigma_1)^2 + (\sigma_2)^2} \tag{52}$$

where σ_1 and σ_2 are the principle stress components of stress $\sigma = \begin{bmatrix} \sigma_{11} & \sigma_{12} \\ \sigma_{12} & \sigma_{22} \end{bmatrix}$.

Note for simplification purpose, the overall effective strain and stress in Fig. 6 are marked as ε and σ respectively. From Fig. 6(b) we can observe a distinct localization band with width of about 20mm.

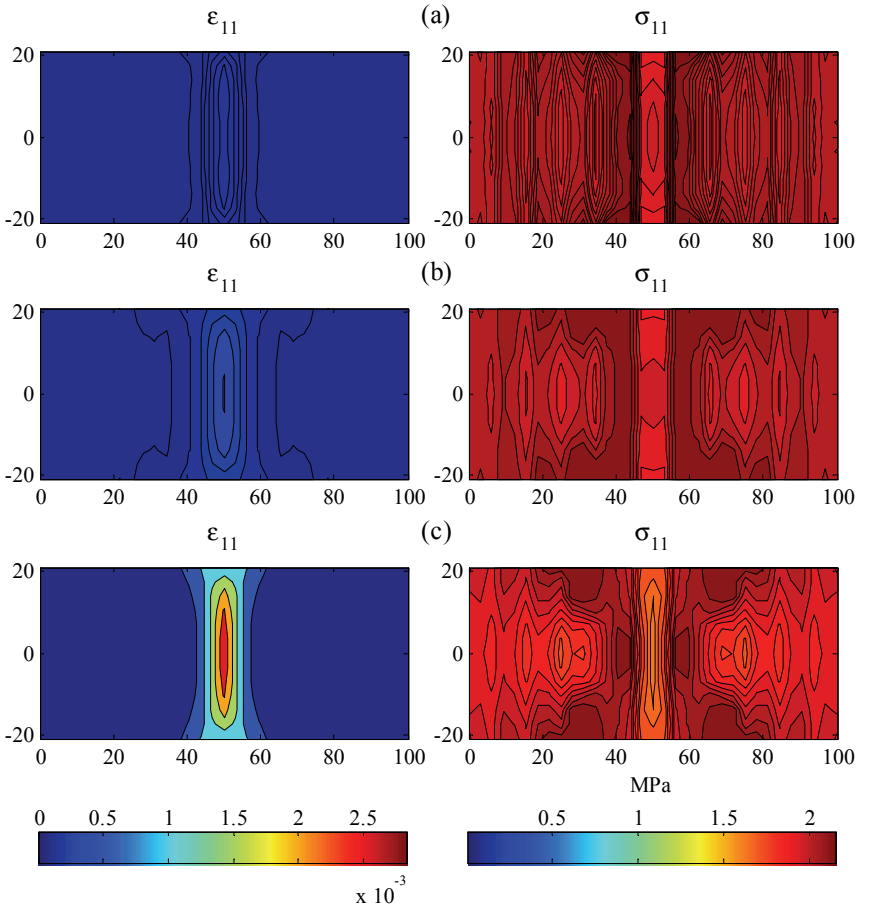

Figure 4: Evolution of axial strain ε_{11} and stress σ_{11} contours at three stages: (a) pre-peak stage, part of nonlinear (b) peak stage, nonlinear (c) post-peak failure stage, nonlinear.

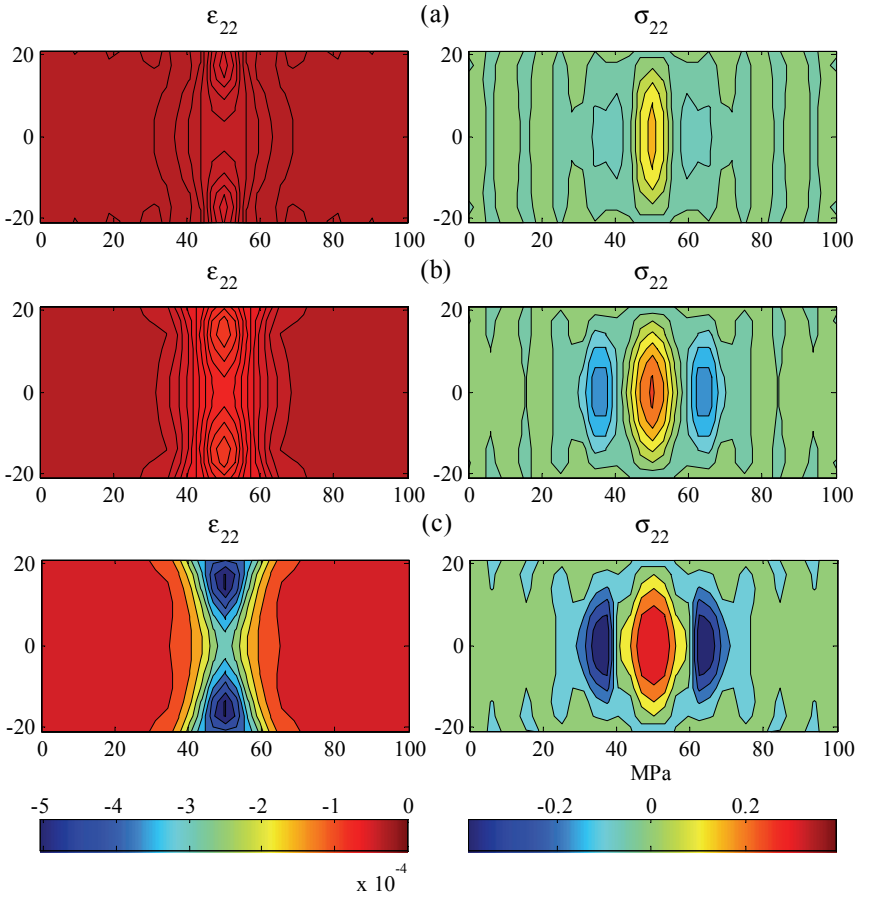

Figure 5: Evolution of axial strain ε_{22} and stress σ_{22} contours at three stages: (a) pre-peak stage, part of nonlinear (b) peak stage, nonlinear (c) post-peak failure stage, nonlinear.

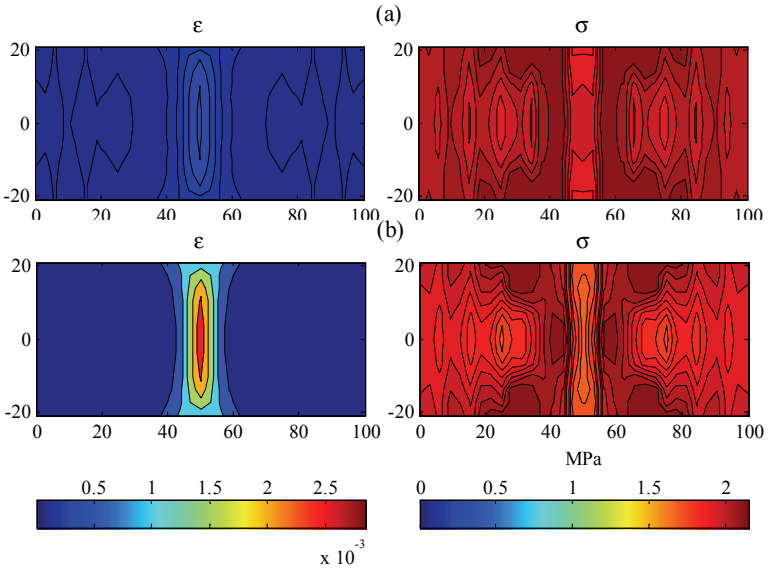

Figure 6: Evolution of the overall effective strain ε and stress σ contours at (a) peak stage, nonlinear (b) post-peak failure stage, nonlinear.

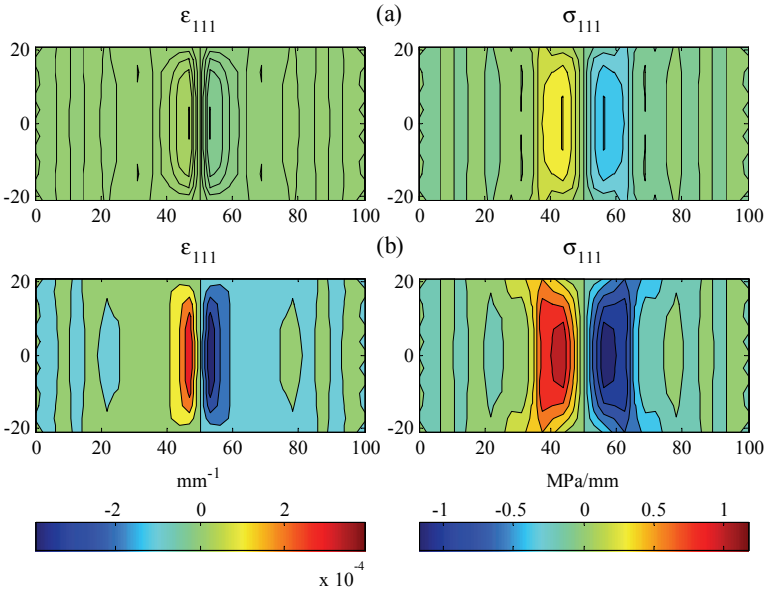

Figure 7: Evolution of higher-order strain ε_{111} and higher-order stress σ_{111} contours at (a) peak stage, nonlinear (d) post-peak failure stage, nonlinear.

Fig. 7 gives the contours of the higher-order strain ε_{111} and conjugated higher-order stress σ_{111} corresponding to the gradients of the horizontal strain ε_{11} and stress σ_{11} with respect to x direction at the peak and failure stages respectively. At the initial stage of loading the higher-order strain are negligible. However as the strains localize within the imperfection, strain gradients develop in their proximity. At peak axial stress stage, two strain gradient bands with mirror symmetry form on the either side of the imperfection as shown in Fig. 7(a). At failure, shown in Fig. 7(b), bands of large strain gradients are present in the immediate neighborhood of the rupture while the rest of the material experiences zero strain gradients which are consistent with the strain and stress profiles shown in Fig. 4(c).

Similarly, the contours of the higher-order strain ε_{222} and higher-order stress σ_{222} corresponding to the gradients of the vertical strain and stress are plotted in Fig. 8 at the peak and failure stages.

Fig. 9 further illustrates the details of the evolution of damage and strain localization by plotting the damage function, ω (Fig. 9(a)), and axial strain, ε_{11}(Fig. 9(b)), along the horizontal central axis over all the loading steps. We note from these figures that as the damage is initiated a localized strain zone begins to emerge within the imperfection. This localized zone grows till we reach the peak stress. Beyond peak stress the localization zone is confined to an unchanging narrow band as shown in Fig. 9(b).

4.1.2 Example 1 – Discretization independency

To validate the mesh objectivity of the proposed higher-order gradient model, results from two different discretizations consisting of 33×13 nodes and 41×15 nodes were compared. All other parameters are kept same as that described in the previous section. Fig. 10 shows the computed damage profile along the horizontal central axis at rapture for the two discretizations. We note that a constant damage width and nearly identical solutions are obtained upon mesh refinement, indicating that the solutions from current method are independent of dicretization size.

4.1.3 Example 1 – Effect of internal length scale parameter

The effect of internal length scale parameter r on softening behavior of the beam can be observed from the damage profiles in Fig. 11 for three different r=1.5mm, 2mm and 3mm, respectively. With the increase of internal length parameter, the localization zone becomes wider which illustrates that the width of localization band is directly governed by the internal length scale as has been widely reported by researchers, such as, Pamin (1994), de Borst and Sluys (1991) and Chang, Askes and Sluys (2002).

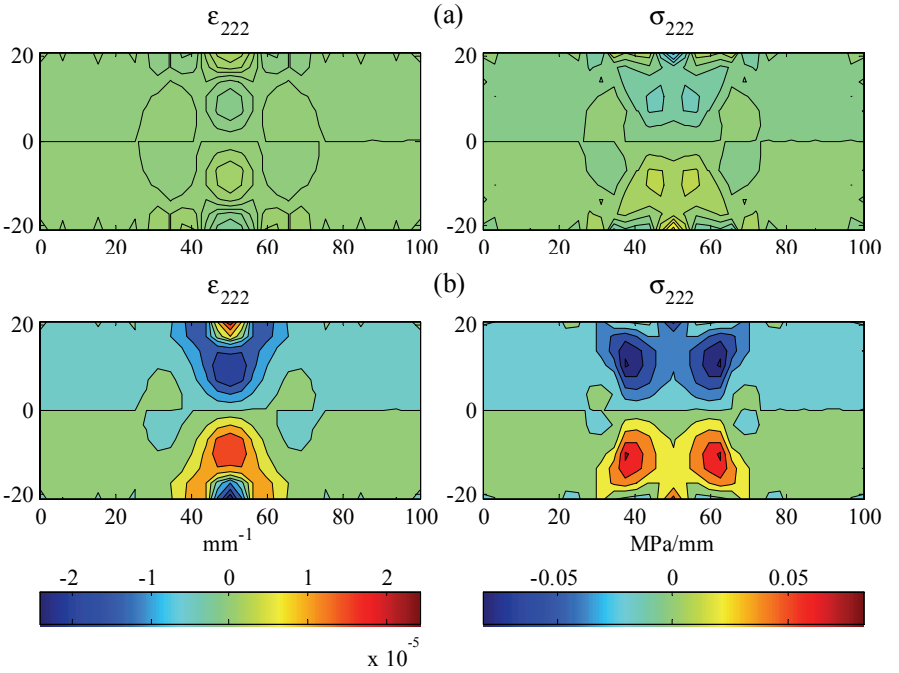

Figure 8: Evolution of higher-order strain ε_{222} and higher-order stress σ_{222} contours at (a) peak stage, nonlinear (d) post-peak failure stage, nonlinear.

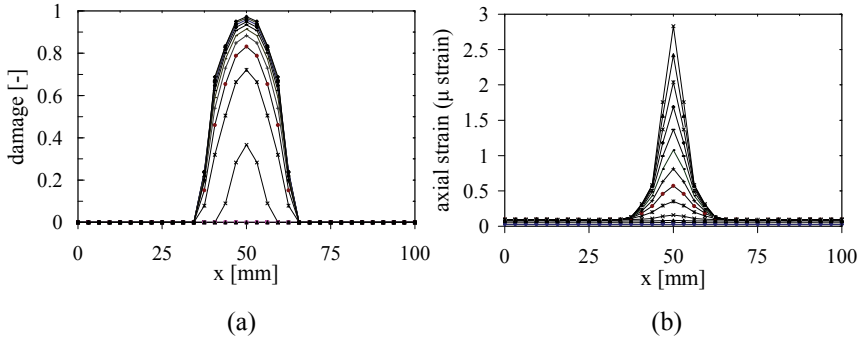

Figure 9: Evolution of (a) damage ω and (b) axial strain ε_{11} along the horizontal central axis over all the loading steps (33×13 nodes, ν=0.25, r=1.5mm)

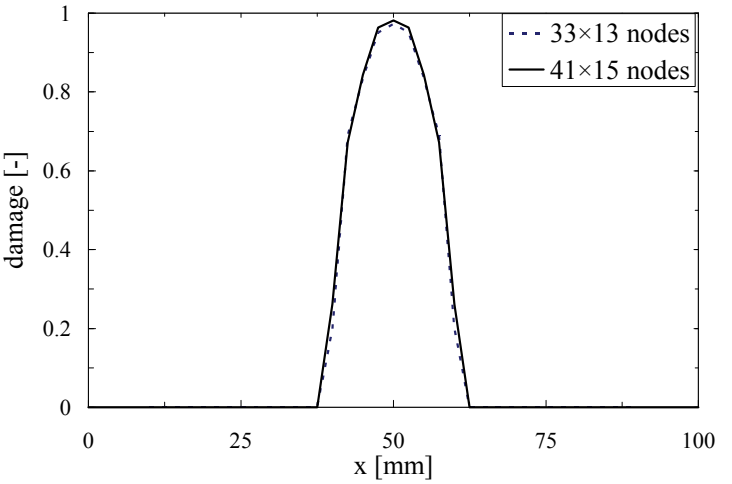

Figure 10: Comparison of damage profile along the horizontal central axis of the plate model with two different nodal layouts

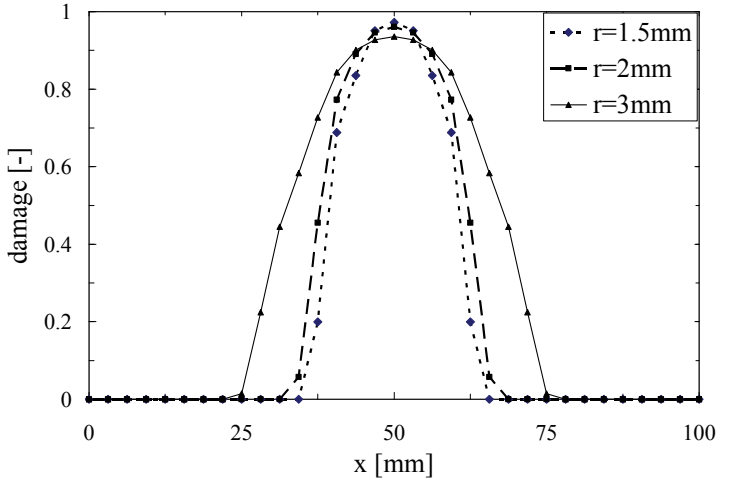

Figure 11: Comparison of damage profile along the horizontal central axis of the plate model for three different values of r.

4.2 Example 2 – Plate with an internal imperfection

Example 1 considered that the imperfection zone is located along the entire section of the plate such that the tensile deformation dominates the fracture process. In example 2, the formation of shear band is investigated originating from an internal square imperfection of side=10mm, placed at the center of the plate as shown in Fig.12. All the other parameters and material properties are taken to be the same as that for example 1. The boundary conditions are also imposed in the same manner as in example 1.

Fig.13 shows the contours of the overall effective strain and the effective stress corresponding to the peak-stress stage and failure stage. At the initial stages of loading, the strain/stress fields are uniformly distributed and strain gradients are absent. At peak-stress stage, an 'x' shaped shear band emerges as shown in Fig. 13(a) which grows in magnitude until failure as shown in Fig. 13(b).

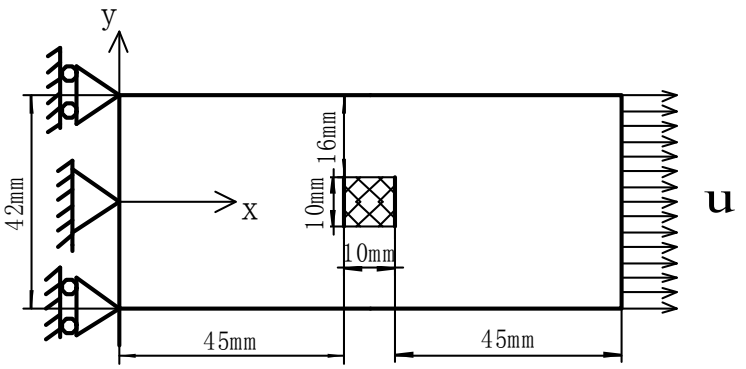

Figure 12: Plate model with an internal imperfection – geometry and loading conditions.

Figs. 14 and 15 show the contours of the overall effective higher-order strain gradients as well as the conjugates of stress gradients with respect to x and y direction respectively.

5 Summary

This paper has presented a higher order stress-strain theory for damage modeling of strain softening materials. In comparison to other gradient theories, the presented higher order theory considers strain gradients and their conjugate higher-order stress. The main contributions of this paper can be summarized as follows:

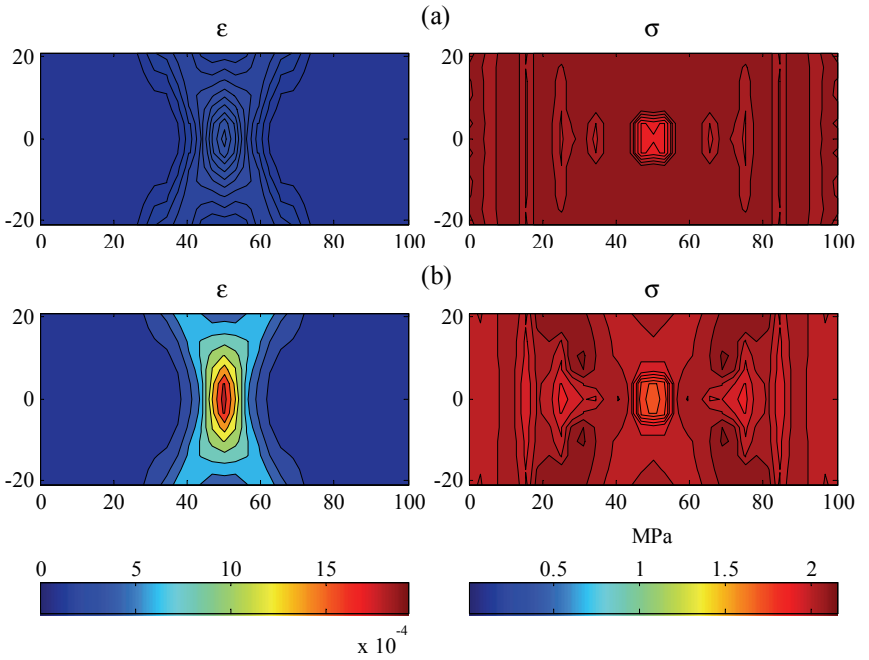

Figure 13: Evolution of the overall effective strain ε and stress σ contours at (a) peak stage, nonlinear (b) post-peak failure stage, nonlinear.

- Derivation of constitutive coefficients for higher-order stress-strain law using a granular media approach that connects the local inter-granular properties and particle size to the macroscopic properties.
- Derivation of the governing equations and their weak form for the higher-order theory in a tensorial form for application to multi-dimensional problems.
- Implementation of the derived theory into a mesh free EFG formulation for the discretization of the governing equations.
- Linearization of the derived discrete equations for numerical simulations.

Since, the constitutive coefficients are derived by considering the underlying physical configuration of the material the internal length scale parameter is naturally incorporated. This length scale parameter acts as a localization limiter in the numerical solutions as has been previously discussed by Larsy and Belytschko (1988). The

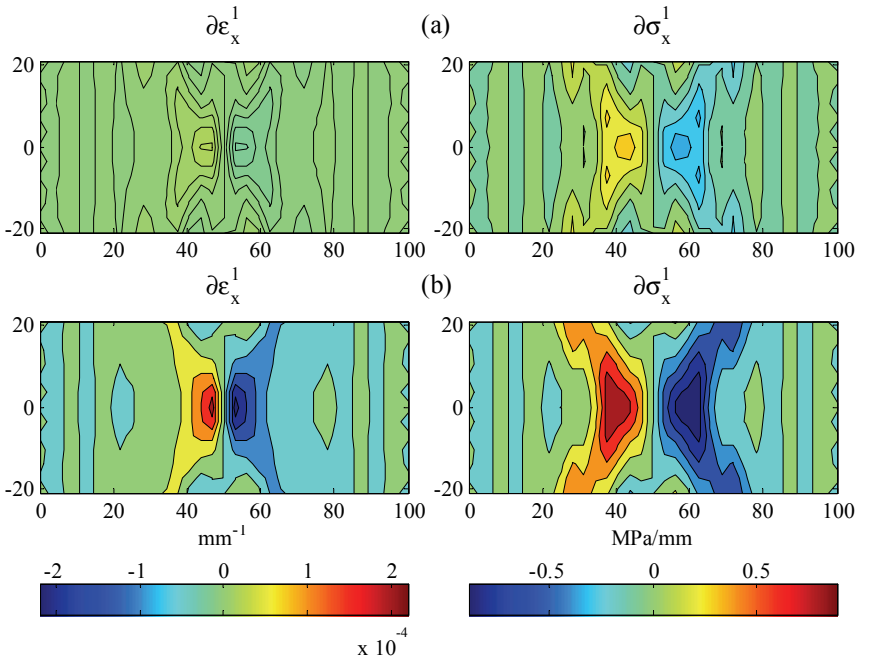

Figure 14: Evolution of the overall effective first-order strain gradient and conjugate stress gradient contours in x-direction at (a) peak stage, nonlinear (b) post-peak failure stage, nonlinear.

higher-order gradient models are discretized via EFG method combining penalty method for the enforcement of essential boundary conditions. The discrete equations are then linearized using Talyor series expansions. The EFG method offers the advantage of incorporating approximation functions with high order of continuity without increasing the problem size.

Two examples of 2-D plates with different imperfections have been numerically analyzed to verify the applicability of the derived model to strain localization. The proposed model can realistically capture the damage process with strain softening phenomenon. Mesh-objectivity is also achieved through the addition of higher-order gradient terms and the use of EFG method. The effect of the internal length scale parameter on the size of the localization band has also been studied. Stable and converged results were obtained for the examples presented in this paper. In our future studies, we will further evaluate the effects of internal length scale parameter on the stability of this approach. We will also apply this approach to investigate the similarities between the predicted strains and strain gradient fields

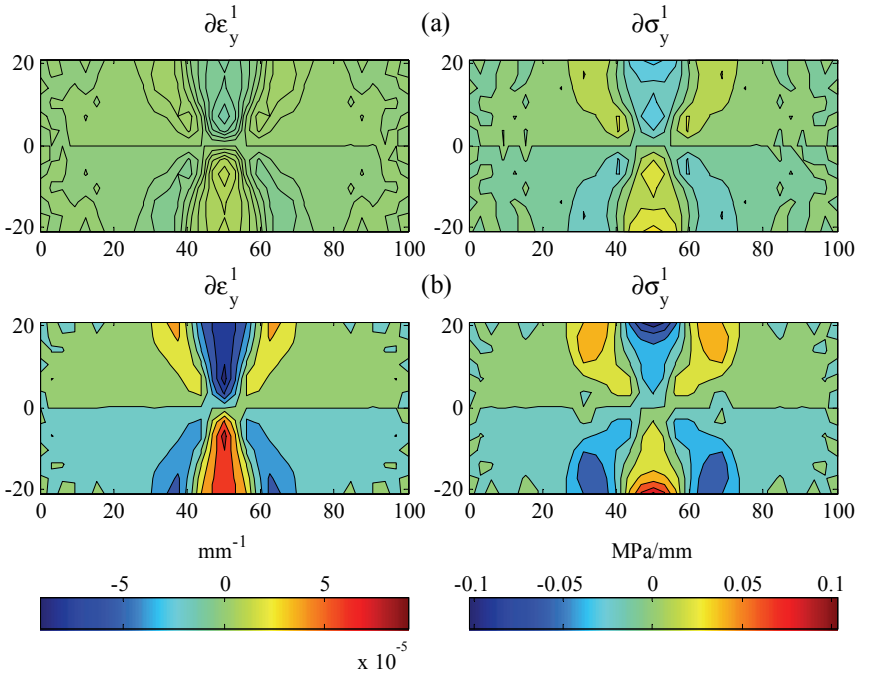

Figure 15: Evolution of the overall effective first-order strain gradient and conjugate stress gradient contours in y-direction at (a) peak stage, nonlinear (b) post-peak failure stage, nonlinear.

and those observed in experiments or atomic simulations performed on brittle materials, such as ceramics and geomaterials. The proposed higher-order theory will also be implemented into the MLPG discretization in the future work.

References

Altan, B. S.; Aifantis, E. C. (1997): On some aspects in the special theory of gradient elasticity. *Journal of the Mechanical Behavior of Materials*, vol. 8, pp. 231-282.

Askes, H.; Pamin, J.; de Borst, R. (2000): Dispersion analysis and element-free Galerkin solutions of second- and fourth-order gradient enhanced damage models. *International Journal for Numerical Methods in Engineering*, vol.49, pp. 811–832.

Atluri, S.N.; Zhu, T. (1998): A new Meshless Local Petrov-Galerkin (MLPG) approach in computational mechanics. *Computational Mechanics*, vol. 22, pp. 117-127.

Atluri, S.N., and Shen, S. (2002): *The Meshless Local Petrov-Galerkin (MLPG) Method*, Tech Science Press.

Bažant, Z.P. (1976): Instability, ductility, and size effect in strain-softening concrete. *Journal of the Engineering Mechanics Division*, vol. 102, no. 2, pp. 331-344.

Bažant, Z.P.; Belytschko, T.; Chang, T.P. (1984): Continuum theory for strain-softening. *Journal of Engineering Mechanics*, vol.110, no.2, pp. 666-1692.

Bažant, Z.P.; Pijaudier-Cabot, G. (1988): Nonlocal continuum damage, localization instability and convergence. *Journal of Applied Mechanics*, vol.55, pp. 287-293.

Belytschko, T.B.; Bažant, Z.P.; Hyun, Y.W.; Chang, T.P. (1986): Strain-softening materials and finite-element solutions. *Computers and Structures*, vol.23, no.2, pp.163-180.

Belytschko, T.; Gu, L.; Lu, Y.Y. (1994): Fracture and crack growth by element free Galerkin methods. *Modeling and Simulation in Materials Science and Engineering*, vol.2, no. 3A, pp. 519-534.

Belytschko, T.; Lu, Y.Y.; Gu,. L. (1994): Element-free Galerkin methods. *International Journal for Numerical Methods in Engineering*, vol.37, no.2, pp.229-256.

Belytschko, T.; Lu, Y.Y.; Gu, L. (1995): Crack propagation by element-free Galerkin methods. *Engineering Fracture Mechanics*, vol.51, no. 2, pp. 295-315.

Belytschko, T.; Lu, Y.Y.; Gu, L.; Tabbara, M. (1995): Element-free Galerkin methods for static and dynamic fracture. *International Journal of Solids and Structures*, vol. 32, no. 17-18, pp. 2547-2570.

Belytschko, T.; Tabbara, M. (1996): Dynamic fracture using element-free Galerkin methods. *International Journal for Numerical Methods in Engineering*, vol.39, pp.923-938.

Chang, C.S.; Askes, H.; Sluys, L.J. (2002): Higher-order strain/higher-order stress gradient models derived from a discrete microstructure, with application to fracture. *Engineering Fracture Mechianics*, vol. 69, pp. 1907-1924.

Chang, C.S.; Gao, J. (1995): Second-gradient constitutive theory for granular material with random packing structure. *International Journal of Solids and Structures*, vol. 32, no. 16, pp. 2279-2293.

Chang, C.S.; Gao, J. (1997): Wave propagation in granular rod using high-gradient theory. *ASCE: Journal of Engineering Mechanics*, vol. 123, pp. 52-59.

Chang, C.S.; Gao, J.; Zhong, X. (1998): High-gradient modeling for love wave propagation in geological materials. *ASCE: Journal of Engineering Mechanics*, vol. 124, pp. 1354-1359.

Chang, C.S.; Liao, C.L. (1990): Constitutive relation for a particulate medium with the effect of particle rotation. *International Journal of Solids and Structures*, vol. 26, no. 4, pp. 437-453.

Chang, C.S.; Ma, L. (1990): Modeling of discrete granulates as micropolar continua. *Journal of Engineering Mechanics*, vol. 116, no. 12, pp. 2703-2721.

Chang, C.S.; Misra, A. (1990): Packing structure and mechanical properties of granulates. *ASCE: Journal of Engineering Mechanics*, vol. 116, no. 5, pp. 1077-1093.

Chang, C.S.; Wang, T.K.; Sluys, L.J.; van Mier, J.G.M. (2002a): Fracture modeling using a micro-structural mechanics approach-¢ñ.Theory and formulation. *Engineering Fracture Mechanics*, vol.69, pp.1941-1958.

Chang, C.S.; Wang, T.K.; Sluys, L.J.; van Mier, J.G.M. (2002b): Fracture modeling using a micro-structural mechanics approach-¢ò.Finite Element Analysis. *Engineering Fracture Mechanics*, vol.69, pp.1959-1976.

Chen, J.S.; Wu, C.T.; Belytschko, T. (2000): Regularization of material instabilities by meshfree approximations with intrinsic length scales. *International Journal for Numerical Methods in Engineering*, vol.47, pp. 1303-1322.

de Borst, R.; Mühlhaus, H.B. (1992): Gradient-dependent plasticity: Formulation and algorithmic aspects. *International Journal for Numerical Methods in Engineering*, vol. 35, pp. 21-39.

de Borst, R.; Pamin, J.; Peerlings, R.H.J.; Sluys, L.J. (1995): On gradient-enhanced damage and plasticity models for failure in quasi-brittle and frictional materials. *Computational Mechanics*, vol. 17, no. 1-2, pp. 130-142.

de Borst, R.; Sluys, L.J. (1991): Localization in a Cosserat continuum under static and dynamic loading conditions. *Computer Methods in Applied Mechanics and Engineering*, vol. 90, pp. 805-827.

de Borst, R.; Sluys, L.J.; Mühlhaus, H.B.; Pamin, J. (1993): Fundamental issues in finite element analyses of localization of deformation. *Engineering Computations*, vol. 10, pp. 99-121.

de Vree, J.H.P.; Brekelmans, W.A.M.; van Gils, M.A.J. (1995): Comparison of nonlocal approaches in continuum damage mechanics. *Computers and Structures*, vol.55, pp. 581-588.

Fleck, N.A.; Hutchinson, J.W. (1997): Strain gradient plasticity. *Advances in Applied Mechanics*, vol. 33, pp. 295-361.

Frantziskonis, G.; Desai, C.S. (1987): Analysis of a strain softening constitutive model. *International Journal of Solids and Structures*, vol.23, no.6, pp 751-767.

Jirásek, M. (1998): Element-free Galerkin method applied to strain-softening ma-

terials, in: R. de Borst et al. (Eds.), Proceedings of EURO-C, *International Conference Computational Modelling of Concrete Structures*, vol. 1, A.A. Balkema, Rotterdam/Brookfield, pp. 311–319.

Kroner, E. (1967): Elasticity theory of materials with long range cohesive forces. *Intational Journal of Solids and Structures*, vol.3, pp.731-742.

Krysl P.; Belytschko, T. (1997): Propagation of 3D cracks by the element free Galerkin method. *Fourth U.S. National Congress on Computational Mechanics, San Francisco.*

Lasry, D.; Belytschko, T. (1988): Localization limiters in transient problems. *International Journal of Solids and Structures*, vol.24, no.6, pp. 581-597.

Liu, G. R.; Gu, Y.T. (2005): *An Introduction to Meshfree Methods and Their Programming.* Dordrecht ; New York : Springer.

Lu, Y.Y.; Belytschko, T.; Tabbara, M. (1994): Element-free Galerkin methods for wave propagation and dynamic fracture. *Computer methods in Applied Mechanics and Engineering*, vol.126, no. 1-2, pp. 131-153.

Mindlin, R.D. (1969): Microstructure in linear elasticity. *Archive for Rational Mechanics and Analysis*, vol.16, no.1, pp. 51-78.

Misra, A.; Ouyang, L.; Chen, J.; Ching, W.Y. (2007): *Ab Initio* calculations of strain fields and failure patterns in silicon nitride intergranular glassy films. *Philosophical Magazine*, vol. 87, no. 25, pp. 3839-3852.

Mühlhaus, H.B.; Oka, F. (1996): Dispersion and wave propagation in discrete and continuous models for granular materials. *International Journal of Solids and Structures*, vol. 33, pp. 2841-2858.

Murakami, H.; Kendall, D.M.; Valanis, K.C. (1993): A nonlocal elastic damage theory: Mesh-Insensitivity under strain softening. *Computers and Structures*, vol.48, no.3, pp.415-422.

Needleman, A. (1988): Material rate dependence and mesh sensitivity in localization problems. *Computer Methods in Applied Mechanics and Engineering*, vol.67, pp.69-85.

Nemes, J.A.; Spéciel, E. (1996): Use of a rate-dependent continuum damage model to describe strain-softening in laminated composites. *Computers and Structures*, vol.58, no. 6, pp. 1083-1092.

Pamin, J. (1994): Gradient-dependent plasticity in numerical simulation of localization phenomena. *PhD thesis, Delft University of Technology*, The Netherlands.

Pamin, J.; Askes, H.; de Borst, R. (2001): Gradient regularization and EFG discretization of the plastic flow theory, in: K.-U. Bletzinger, K. Schweizerhof, W.A. Wall (Eds.), *Conference on Trends in Computational Structural Mechanics*,

CIMNE, Barcelona, pp.179–188.

Pamin, J.; Askes, H.; de Borst, R. (2003): Two gradient plasticity theories discretized with the element-free Galerkin method. *Computer Methods in Applied Mechanics and Engineering*, vol. 192, pp.2377–2403.

Peerlings, R.H.J.; de Borst, R.; Brekelmans, W.A.M.; de Vree, J.H.P. (1996): Gradient enhanced damage for quasi-brittle materials. *International Journal for Numerical Methods in Engineering*, vol.39, no.19, pp. 3391-3403.

Pietruszczak, St.; Mroz, Z. (1981): Finite element analysis of deformation of strain-softening materials. *International Journal for Numerical Methods in Engineering*, vol. 17, pp. 327-334.

Reddy, J.N. (2005): *An introduction to finite element method (3^{rd} Edition).* McGraw-Hill Science/Engineering/Math.

Sandler, I.S. (1984): Strain softening for static and dynamic problems. *ASME Winter Annual Meeting, Symp. On constitutive equations: Micro, Macro and Computational Aspects*, CEQ, New Orleans, pp. 217-231.

Sluys, L.J. (1992): Wave propagation, localization and dispersion in softening solids. *Ph.D.thesis, Delft University of Technology*, The Netherlands.

Sluys, L.J.; Cauvern, M.; de Borst, R. (1995): Discretization influence in strain-softening problems. *Engineering computations*, vol.12, pp, 209-228.

Sluys, L.J.; de Borst, R. (1992): Wave-propagation and localization in a rate-dependent cracked medium model formulation and one-dimensional examples. *International Journal of Solids and Structures*, vol.29. pp. 2945-2958.

Sluys, L.J.; de Borst, R.; Mühlhaus, H.B. (1993): Wave propagation, localization and dispersion in a gradient-dependent medium. *International Journal of Solids and Structures*, vol. 30, pp. 1153-1171.

Steinmann, P. (1994): An improved FE expansion for micropolar localization analysis. *Communications in Numerical Methods in Engineering*. vol.10, no.12, pp.1005-1012.

Suiker, A.S.J.; de Borst, R.; Chang, C.S. (2001a): Micro-mechanical modeling of granular material, part 1-Derivation of a second-gradient micro-polar constitutive theory. *Acta Mechanica*, vol. 149, no. 1-4, pp. 161-180.

Suiker, A.S.J.; de Borst, R.; Chang, C.S. (2001b): Micro-mechanical modeling of granular material. part 2-Plane wave propagation in infinite media. *Acta Mechanica*, vol. 149, no. 1-4, pp. 181-200.

Tang, Z.; Shen, S.; Atluri, S.N. (2003): Analysis of materials with strain-gradient effects: A Meshles Local Petrov-Galerkin (MLPG) approach, with nodal displacements only. *Computer Modeling in Engineering and Sciences*, vol. 4, no. 4, pp.

177-196.

Triantafyllidis, N.; Aifantis, E.C. (1986): A gradient approach to localization of deformation. I. Hyperelastic materials. *Journal of Elasticity*, vol. 16, no. 3, pp. 225-237.

Triantafyllidis, N.; Bardenhagen, S. (1993): On higher order gradient continuum theories in 1-D nonlinear elasticity. Derivation from and comparison to the corresponding discrete models. *Journal of Elasticity*, vol. 33, pp. 259-293.

Valanis, K.C. (1991): A global damage theory and the hyperbolicity of the wave problem. *ASME Journal of applied Mechanics*, vol. 58, no. 2, pp.311-316.

van Mier, J.G.M., (1984): Strain-softening of concrete under multiaxial loading conditions. *Ph.D.thesis, Eindhoven University of Technology*, The Netherlands.

van Mier, J.G.M., (1986): Multiaxial strain-softening of concrete. *Materials and Structures*, vol.19, pp.190-200.

van Mier, J.G.M.; Shah, S.P.; Arnaud, M.; Balayssac, J.P.; Bascoul, A.; Choi, S.; Dasenbrock, D.; Ferrara, G.; French, C.; Gobbi, M.E.; Karihaloo, B.L.; Konig, G.; Kotsovos, M.D.; Labuz, J.;Lange-Kornbak, D.; Markeset, G.; Pavlovic, M.N.; Simsch, G.; Thienel, K-C.; Turatsinze, A.;Ulmer, M.; van Geel, H.J.G.M.; van Vliet, M.R.A.; Zissopoulos, D. (1997): Strain-softening of concrete in uniaxial compression. *Materials and Structures*, vol. 30, pp.195-209.

Wu, F.H.; Freund, L.B. (1984): Deformation trapping due to thermoplastic instability in one dimensional wave propagation. *Journal of Mechanics and Physics of Solids*, vol.32, no. 2, pp.119-132.

Zhu, T.; Atluri, S.N. (1998): A modified collocation method and a penalty formulation for enforcing the essential boundary conditions in the element free Galerkin method. *Computational Mechanics*, vol. 21, no. 3, pp. 211-222.

Appendix A. Higher-order constitutive constants of isotropic packing structure

We consider a material with an isotropic underlying structure whose fabric parameters are taken as $a_{20} = a_{22} = b_{22} = 0$. Under infinitesimal initial strain, material properties can be represented by two constants, i.e. Young's modulus E and Poisson's ratio ν, and the following relations between material properties and components of contact stiffness can be derived (Chang and Misra (1990); Chang and Gao (1995)):

$$E = a\left(\frac{K_n(2K_n+3K_w)}{3(4K_n+K_w)}\right) \tag{A.1}$$

$$\nu = \frac{K_n - K_w}{4K_n + K_w} \tag{A.2}$$

with $a = 2r^2 N/V$ representing the density of the packing structure.

Eqs.(A.1) and (A.2) can be rearranged to give

$$K_n = \frac{3E}{a(1-2\nu)} \tag{A.3}$$

$$K_w = \frac{3E(1-4\nu)}{a(1-2\nu)(1+\nu)} \tag{A.4}$$

Substituting Eqs.(6), (7) and (20) into (21a) and integrating we arrive at the zeroth-order constitutive constants, C_{ijkl}, as

$$C_{1111} = \frac{a}{15}(3K_n + 2K_w) \tag{A.5}$$

$$C_{1122} = \frac{a}{15}(K_n - K_w) \tag{A.6}$$

$$C_{1212} + C_{1221} = \frac{a}{15}\left(K_n + \frac{3}{2}K_w\right) \tag{A.7}$$

And for this case, the following identities for zeroth-order elastic moduli hold:

$$C_{1111} = C_{2222} \tag{A.8}$$

$$C_{1122} = C_{2211} \tag{A.9}$$

$$C_{1212} = C_{2121} \tag{A.10}$$

Inserting Eqs.(A.3) and (A.4) into Eqs.(A.5)-(A.7), the zeroth-order constitutive coefficients can be related to E and ν to recover the usual relations of isotropic elastic tensor.

$$C_{1111} = \frac{E(1-\nu)}{(1-2\nu)(1+\nu)} \tag{A.11}$$

$$C_{1122} = \frac{E\nu}{(1-2\nu)(1+\nu)} \tag{A.12}$$

$$\frac{1}{2}(C_{1212} + C_{1221}) = \frac{E}{2(1+\nu)} \tag{A.13}$$

By combing Eqs. (6), (7), (20), (21b), (A.3) and (A.4) and using a similar algebra, the components of first-order constitutive constants D_{ijqklm} can be obtained as

$$D_{111111} = \frac{3r^2 E(7-3\nu)}{35(1-2\nu)(1+\nu)} \tag{A.14}$$

$$D_{111122} = \frac{r^2 E(7-13\nu)}{35(1-2\nu)(1+\nu)} \tag{A.15}$$

$$D_{111212} = \frac{3r^2 E\nu}{7(1-2\nu)(1+\nu)} \tag{A.16}$$

$$D_{122122} = \frac{3r^2 E(7-23\nu)}{35(1-2\nu)(1+\nu)} \tag{A.17}$$

where the following relations hold

$$D_{111111} = D_{222222} \tag{A.18}$$

$$D_{111122} = D_{112112} = D_{112121} = D_{121121} = D_{211222} = D_{212212} = D_{212221} = D_{221221} \tag{A.19}$$

$$D_{111212} = D_{111221} = D_{112211} = D_{112222} = D_{121211} = D_{121222} = D_{122212} = D_{122221} \tag{A.20}$$

$$D_{122122} = D_{211211} \tag{A.21}$$

The other elements of C_{ijkl} and D_{ijqklm} are all zero. Note that (1) Eqs.(A.3) and (A.4) provide a useful method for estimating the high-order constitutive constants directly from the Young's modulus and Poisson's ratio without explicitly knowing the numerical values of either the number of contacts N or the representative volume V; and (2) the derived higher-order constitutive coefficients explicitly depend upon the particle radius, r, which functions as a internal length scale parameter.

Appendix B Weak form derivation

To derive the weak form equilibrium equation from Eq. (27) we pre-multiply by test function, δu_i, and integrate over the 2-D domain Ω as

$$\begin{aligned}
&\int_\Omega \delta u_i \{(1-\omega)(C_{iqkl}\frac{\partial^2 u_k}{\partial x_q \partial x_l} - D_{ijqklr}\frac{\partial^4 u_k}{\partial x_r \partial x_j \partial x_q \partial x_l}) \\
&- \frac{\partial \omega}{\partial \varepsilon^0_{mn}}\frac{\partial^2 u_m}{\partial x_q \partial x_n}(C_{iqkl}\frac{\partial u_k}{\partial x_l} - D_{ijqklr}\frac{\partial^3 u_k}{\partial x_r \partial x_j \partial x_l}) \\
&\quad + \frac{\partial \omega}{\partial \varepsilon^0_{mn}}(\frac{\partial^3 u_m}{\partial x_j \partial x_q \partial x_n}D_{ijqklr}\frac{\partial^2 u_k}{\partial x_r \partial x_l} + \frac{\partial^2 u_m}{\partial x_j \partial x_n}D_{ijqklr}\frac{\partial^3 u_k}{\partial x_r \partial x_q \partial x_l})\} d\Omega = 0
\end{aligned} \tag{B.1}$$

The above integration is evaluated through integration by parts as follows:

$$\int_\Omega \delta u_i(1-\omega)C_{iqkl}\frac{\partial^2 u_k}{\partial x_q \partial x_l}d\Omega = \int_{\Gamma_t} \delta u_i(1-\omega)C_{iqkl}\frac{\partial u_k}{\partial x_l}n_q d\Gamma - \int_\Omega \frac{\partial \delta u_i}{\partial x_q}(1-\omega)C_{iqkl}\frac{\partial u_k}{\partial x_l}dxdy + \int_\Omega \delta u_i \frac{\partial \omega}{\partial \varepsilon^0_{mn}}\frac{\partial \varepsilon^0_{mn}}{\partial x_q}C_{iqkl}\frac{\partial u_k}{\partial x_l}dxdy \quad \text{(B.2)}$$

and

$$\int_\Omega \delta u_i(1-\omega)D_{ijqklr}\frac{\partial^4 u_k}{\partial x_r \partial x_j \partial x_q \partial x_l}d\Omega = \int_{\Gamma_t} \delta u_i(1-\omega)D_{ijqklr}\frac{\partial^3 u_k}{\partial x_r \partial x_j \partial x_l}n_q d\Gamma - \int_\Omega (\frac{\partial \delta u_i}{\partial x_q}(1-\omega)D_{ijqklr}\frac{\partial^3 u_k}{\partial x_r \partial x_j \partial x_l} + \delta u_i \frac{\partial \omega}{\partial \varepsilon^0_{mn}}\frac{\partial \varepsilon^0_{mn}}{\partial x_q}D_{ijqklr}\frac{\partial^3 u_k}{\partial x_r \partial x_j \partial x_l})dxdy \quad \text{(B.3)}$$

Substituting Eqs.(B.2) and (B.3) into Eq.(B.1) and using some algebra we get

$$\int_\Omega \frac{\partial \delta u_i}{\partial x_q}(1-\omega)(C_{iqkl}\frac{\partial u_k}{\partial x_l} - D_{ijqklr}\frac{\partial^3 u_k}{\partial x_r \partial x_j \partial x_l})dxdy - \int_\Omega \delta u_i \frac{\partial \omega}{\partial \varepsilon^0_{mn}}D_{ijqklr}(\frac{\partial^3 u_m}{\partial x_j \partial x_q \partial x_n}\frac{\partial^2 u_k}{\partial x_r \partial x_l} + \frac{\partial^2 u_m}{\partial x_j \partial x_n}\frac{\partial^3 u_k}{\partial x_r \partial x_q \partial x_l})dxdy = \int_{\Gamma_t} \delta u_i(1-\omega)(C_{iqkl}\frac{\partial u_k}{\partial x_l} - D_{ijqklr}\frac{\partial^3 u_k}{\partial x_r \partial x_j \partial x_l})n_q d\Gamma \quad \text{(B.4)}$$

Further integration by parts is carried out for the higher-order integrals in Eq.(B.4) as

$$\int_\Omega \frac{\partial \delta u_i}{\partial x_q}(1-\omega)D_{ijqklr}\frac{\partial^3 u_k}{\partial x_r \partial x_j \partial x_l}dxdy = \int_{\Gamma_t} \frac{\partial \delta u_i}{\partial x_q}(1-\omega)D_{ijqklr}\frac{\partial^2 u_k}{\partial x_r \partial x_l}n_j d\Gamma - \int_\Omega \frac{\partial^2 \delta u_i}{\partial x_q \partial x_j}(1-\omega)D_{ijqklr}\frac{\partial^2 u_k}{\partial x_r \partial x_l}dxdy + \int_\Omega \frac{\partial \delta u_i}{\partial x_q}\frac{\partial \omega}{\partial \varepsilon^0_{mn}}\frac{\partial^2 u_m}{\partial x_j \partial x_n}D_{ijqklr}\frac{\partial^2 u_k}{\partial x_r \partial x_l}dxdy \quad \text{(B.5)}$$

and

$$\int_\Omega \delta u_i \frac{\partial \omega}{\partial \varepsilon^0_{mn}}D_{ijqklr}\frac{\partial^2 u_m}{\partial x_j \partial x_n}\frac{\partial^3 u_k}{\partial x_r \partial x_q \partial x_l}dxdy = \int_{\Gamma_t} \delta u_i \frac{\partial \omega}{\partial \varepsilon^0_{mn}}D_{ijqklr}\frac{\partial^2 u_m}{\partial x_j \partial x_n}\frac{\partial^2 u_k}{\partial x_r \partial x_l}n_q d\Gamma - \int_\Omega (\frac{\partial \delta u_i}{\partial x_q}\frac{\partial^2 u_m}{\partial x_j \partial x_n}\frac{\partial^2 u_k}{\partial x_r \partial x_l} + \delta u_i \frac{\partial^3 u_m}{\partial x_j \partial x_n \partial x_q}\frac{\partial^2 u_k}{\partial x_r \partial x_l})D_{ijqklr}\frac{\partial \omega}{\partial \varepsilon^0_{mn}}dxdy \quad \text{(B.6)}$$

Inserting Eqs.(B.5) and (B.6) into Eq.(B.4), the weak form can be written as

$$\begin{aligned}
&\int_\Omega \frac{\partial \delta u_i}{\partial x_q}(1-\omega)C_{iqkl}\frac{\partial u_k}{\partial x_l}dxdy+\int_\Omega \frac{\partial^2 \delta u_i}{\partial x_q \partial x_j}(1-\omega)D_{ijqklr}\frac{\partial^2 u_k}{\partial x_r \partial x_l}dxdy \\
&=\int_{\Gamma_t}\frac{\partial \delta u_i}{\partial x_q}(1-\omega)D_{ijqklr}\frac{\partial^2 u_k}{\partial x_r \partial x_l}n_j d\Gamma \\
&+\int_{\Gamma_t}\delta u_i(1-\omega)(C_{iqkl}\frac{\partial u_k}{\partial x_l}-D_{ijqklr}\frac{\partial^3 u_k}{\partial x_r \partial x_j \partial x_l})n_q d\Gamma \\
&\qquad +\int_{\Gamma_t}\delta u_i \frac{\partial \omega}{\partial \varepsilon^0_{mn}}D_{ijqklr}\frac{\partial^2 u_m}{\partial x_j \partial x_n}\frac{\partial^2 u_k}{\partial x_r \partial x_l}n_q d\Gamma
\end{aligned} \tag{B.7}$$

Because

$$\begin{cases}
\sigma^0_{iq}=(1-\omega)C_{iqkl}\varepsilon^0_{kl}=(1-\omega)C_{iqkl}\frac{\partial u_k}{\partial x_l} \\
\sigma^1_{ijq}=(1-\omega)D_{ijqklr}\varepsilon^1_{klr}=(1-\omega)D_{ijqklr}\frac{\partial^2 u_k}{\partial x_l \partial x_r} \\
\frac{\partial \sigma^1_{ijq}}{\partial x_j}=(1-\omega)D_{ijqklr}\frac{\partial^3 u_k}{\partial x_l \partial x_r \partial x_j}-\frac{\partial \omega}{\partial \varepsilon^0_{mn}}\frac{\partial^2 u_m}{\partial x_n \partial x_j}D_{ijqklr}\frac{\partial^2 u_k}{\partial x_l \partial x_r}
\end{cases} \tag{B.8}$$

Eq.(B.7) can be recast to the final weak form equilibrium equation as

$$\begin{aligned}
&\int_\Omega \frac{\partial \delta u_i}{\partial x_q}(1-\omega)C_{iqkl}\frac{\partial u_k}{\partial x_l}dxdy+\int_\Omega \frac{\partial^2 \delta u_i}{\partial x_q \partial x_j}(1-\omega)D_{ijqklr}\frac{\partial^2 u_k}{\partial x_r \partial x_l}dxdy \\
&\qquad =\int_{\Gamma_t}\frac{\partial \delta u_i}{\partial x_q}\sigma^1_{ijq}n_j d\Gamma+\int_{\Gamma_t}\delta u_i(\sigma^0_{iq}-\frac{\partial \sigma^1_{ijq}}{\partial x_j})n_q d\Gamma
\end{aligned} \tag{B.9}$$